PEGylated Micelle Nanoparticles Encapsulating a Non-Fluorescent Near-Infrared Organic Dye as a Safe and Highly-Effective Photothermal Agent for In Vivo Cancer Therapy

Liang Cheng, Weiwei He, Hua Gong, Chao Wang, Qian Chen, Zhengping Cheng, and Zhuang Liu**

Photothermal therapy (PTT), as a minimally invasive and highly effective cancer treatment approach, has received widespread attention in recent years. Tremendous effort has been devoted to explore various types of photothermal agents with high near-infrared (NIR) absorbance for PTT cancer treatment. Despite many exciting progresses in the area, effective yet safe photothermal agents with good biocompatibility and biodegradability are still highly desired. In this work, a new organic PTT agent based on polyethylene glycol (PEG) coated micelle nanoparticles encapsulating a heptamethine indocyanine dye IR825 is developed, showing a strong NIR absorption band and a rather low quantum yield, for in vivo photothermal treatment of cancer. It is found that the IR825–PEG nanoparticles show ultra-high in vivo tumor uptake after intravenous injection, and appear to be an excellent PTT agent for tumor ablation under a low-power laser irradiation, without rendering any appreciable toxicity to the treated animals. Compared with inorganic nanomaterials and conjugated polymers being explored in PTT, the NIR-absorbing micelle nanoparticles presented here may have the least safety concern while showing excellent treatment efficacy, and thus may be a new photothermal agent potentially useful in clinical applications.

1. Introduction

Photothermal therapy (PTT) is a hyperthermia therapeutic approach that employs heat generated from optical energy to kill cancer cells with high efficiency and minimal invasiveness.[1,2] In typical applications of PTT, photothermal agents with strong optical absorbance, preferably in the tissue-transparent near-infrared (NIR) window (700–900 nm), are generally indispensable. Ideal photothermal agents should exhibit strong and stable NIR absorbance and, thus, are able to effectively convert the absorbed NIR light energy into heat. In addition, the agents used in PTT should be nontoxic and show high tumor-homing ability, to improve therapeutic efficacy without rendering toxic side effects. In recent years, a variety of NIR-absorbing inorganic nanomaterials, such as different gold nanostructures,[3–9] carbon nanomaterials,[2,10–12] palladium nanosheets,[13,14] copper sulfide nanoparticles,[15,16] and tungsten oxide nanowires[17] have been widely explored by many research groups including ours as photothermal agents for PTT ablation of cancer cells in vitro and in vivo. Although many of the above materials have already shown high efficacies for PTT treatment of cancers in pre-clinical animal experiments, most of these currently used inorganic photothermal agents are non-biodegradable and would retain in the body for long periods of time, preventing their further application in clinical cancer treatment due to the potential long-term toxicity concern.[18]

Recently, significant attentions have been paid to the development of NIR-absorbing organic materials as photothermal agents in PTT cancer treatment. A number of conjugated polymers with appropriate aromatic structures exhibit rather large NIR absorption cross-sections. In several recent studies, we and others have developed NIR-absorbing nano-agents based on conjugated polymers, such as polyaniline, polypyrrole, and poly-(3, 4-ethylenedioxythiophene):poly (4-styrenesulfonate) (PEDOT:PSS) which, after appropriate surface modification, could be used for highly effective in vivo PTT treatment of cancer in animal experiments.[19–22] Despite the encouraging PTT therapeutic effects obtained using those polymeric nanoparticles, the biodegradation behaviors of conjugated polymers remain unclear. Porphyrin-lipid, or porphysomes, is another type of new PTT nano-agent currently under investigation.[23] However, the absorbance peak of porphyrin compounds

Dr. L. Cheng, H. Gong, C. Wang, Q. Chen
Prof. Z. Liu
Jiangsu Key Laboratory for Carbon-Based Functional Materials & Devices
Institute of Functional Nano & Soft Materials Laboratory (FUNSOM)
Soochow University
Suzhou, Jiangsu 215123, China
E-mail: zliu@suda.edu.cn
Mr. W. He, Prof. Z. Cheng
Department of Polymer Science and Engineering
Jiangsu Key Laboratory of Advanced Functional Polymer Design and Application
College of Chemistry, Chemical Engineering and Materials Science
Soochow University
Suzhou, Jiangsu 215006, China
E-mail: chengzhenping@suda.edu.cn

DOI: 10.1002/adfm.201301045

locates in the red light region (660–670 nm), which exhibits much lower tissue penetration ability compared to NIR light due to the existence of porphyrin-containing hemochrome in red blood cells.[24] In a few latest reports, several other organic nanomaterials, such as Prussian blue nanoparticles and dopamine-melanin colloidal nanospheres, also showed their possibility to be used as PTT agents.[25,26] Although those materials could absorb NIR light, their peaked absorption is not in the NIR region.

Small organic fluorescent dyes have been extensively studied in past decades, mainly as labeling probes in optical imaging. For example, indocyanine dyes, which could be engineered to acquire strong NIR absorption and emission, have been synthesized and widely used for in vivo fluorescent imaging.[27–29] Among them, indocyanine green (ICG) has been approved by federal drug administration (FDA) for a number of clinical applications.[28,30–32] Besides being used in fluorescent imaging, ICG is also under investigation as a photodynamic therapy agent,[28,31] which produces reactive oxygen species instead of heat to damage cancer cells under light exposure, although the use of ICG for photothermal cancer treatment has also been demonstrated in several recent reports.[33]

Organic dyes with high quantum yields (QY) are generally preferred in fluorescent optical imaging. However, their photothermal efficiency could be low because a part or even a majority of the absorbed optical energy is emitted from those dye molecules as fluorescence instead of heat. Organic dyes with high NIR absorption co-efficients but low QYs, on the other hand, may offer the best photothermal efficiency, since the thermal effect would prevail in the energy dissipation process of those molecules after light excitation. Therefore, in this work, we synthesize a NIR-absorbing heptamethine indocyanine dye, IR825, which shows a super high NIR absorption peak at ≈825 nm and a rather low QY (<0.1%). A polyethylene glycol (PEG) grafted amphiphilic polymer is used to solubilize IR825, forming IR825–PEG micelle nanoparticles with great solubility in water and other physiological solutions. Compared with ICG, IR825–PEG exhibits stronger photothermal effect under 808-nm NIR laser irradiation, and more importantly, dramatically improved photothermal stability. Without showing any appreciable toxicity to cells, IR825–PEG could serve as an effective photothermal agent to destruct cancer cells under NIR light. In vivo animal experiments uncover the ultra-long blood circulation half-life of IR825–PEG. As the result, highly efficient passive tumor accumulation of IR825–PEG is observed, owing to the enhanced permeability and retention (EPR) effect of cancerous tumors. In vivo photothermal therapy is then carried out in a mouse tumor model by intravenous (i.v.) injection of IR825–PEG nanoparticles and laser irradiation of tumors at a low optical power density (0.5 W cm^{-2}), achieving an excellent therapeutic efficacy with 100% of tumor destruction. Moreover, no obvious signal of toxicity is observed on IR825–PEG injected mice as evidenced by both hemological and histological data. Our work presents a new photothermal agent based on nanoparticles of an NIR-absorbing organic dye, which is safe and highly effectively for photothermal cancer treatment.

2. Results and Discussion

A heptamethine indocyanine dye, IR825, which is a lipophilic cation with strong adsorption at 825 nm (in methanol) (**Figure 1**a,b), was synthesized following the procedure described in the experimental section (**Scheme 1**). The structure of IR825 was confirmed by ^{1}H-NMR and high-resolution mass spectrum (HRMS) (Supporting Information, Figure S1). The molar absorption coefficient of IR825 at the peak of 825 nm in methanol was calculated to be 1.145×10^5 $M^{-1}cm^{-1}$. On the other hand, the fluorescence QY of IR825 dye was determined to be <0.1% in methanol, which was much lower than that of ICG[34] (Supporting Information, Figure S2).

As-synthesized IR825 was not water-soluble. We therefore used PEG-grafted poly (maleicanhydride-alt-1-octadecene) (C18PMH–PEG), a biocompatible amphiphilic polymer used in our previous studies to functionalize a variety of inorganic nanomaterials,[35–37] to solubilize IR825 (Figure 1a), forming PEGylated IR825 micelle nanoparticles (IR825–PEG) with excellent stability in physiological solutions (Supporting Information, Figure S3). Compared with IR825 in methanol, IR825–PEG nanoparticles in water showed broadened but slightly reduced NIR absorbance (Figure 1b), and completely quenched fluorescence that was close to the noise level (Supporting Information, Figure S2), likely owing to the intermolecular interactions between IR825 molecules inside the micelle core. Based on images of atomic force microscopy (AFM) and transmission electron microscopy (TEM), the average micelle diameter was ≈25 nm (Figure 1c; Figure S4, Supporting Information), consistent to that measured by dynamic light scattering (DLS) (Figure 1d), even though AFM and TEM imaged nanoparticles in the dried form, while DLS measured the hydrodynamic sizes of nanoparticles in the aqueous solution. With time, the diameter of IR825–PEG nanoparticles in phosphate buffered saline (PBS) remained unchanged, indicating the great stability of those nanoparticles without aggregation (Figure 1d).

We then studied the photothermal properties of our PEGylated IR825 nanoparticles. IR825–PEG solutions with various concentrations at 0.05, 0.1, 0.2, and 0.5 mg mL^{-1} were exposed to an 808-nm NIR laser at a power density of 0.5 W cm^{-2}. Obvious concentration-dependent temperature increases of IR825–PEG solutions were found under laser irradiation, while pure water showed little change (Figure 1e). Compared with ICG, the FDA-approved NIR dye widely explored in photodynamic and photothermal therapies,[28,31,33] IR825–PEG showed an absorbance peak located in the longer wavelength (Figure 1g). Under the 808-nm laser irradiation, the temperature rise of the IR825–PEG solution was higher than that of ICG at the same concentration (Figure 1f). More importantly, IR825–PEG exhibited outstanding photostability under constant laser exposure, without losing its NIR absorbance after 10 min of irradiation (808 nm, 0.5 W cm^{-2}), which, in marked contrast, resulted in nearly complete elimination of ICG NIR absorbance (Figure 1g). The strong and stable photothermal performance of IR825–PEG makes it an encouraging nano-agent for PTT cancer treatment.

To explore the applications of IR825–PEG nanoparticles in biomedicine, we first tested their potential toxicity to several

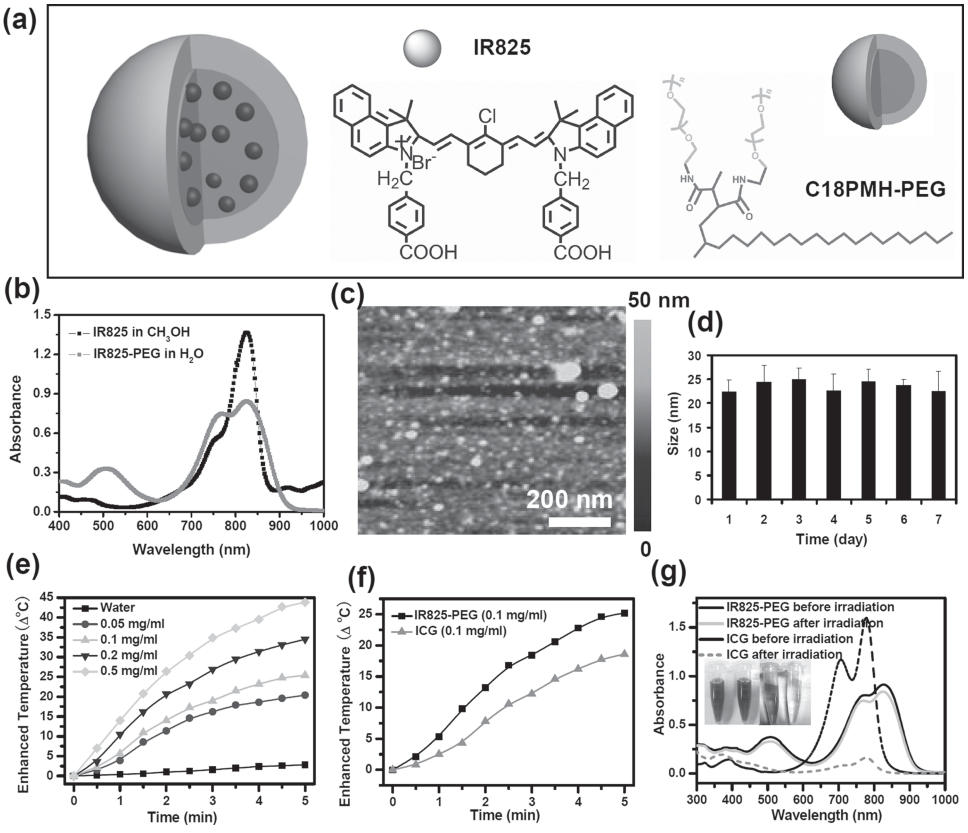

Figure 1. IR825-PEG characterization. a) A scheme showing the composition of IR825–PEG nanoparticles. b) UV-vis-NIR absorbance spectra of IR825 in methanol and IR825–PEG in water. c) An AFM image of IR825–PEG nanoparticles. d) DLS measured diameters of IR825–PEG after being incubated in PBS for different periods. Error bars were based standard deviations (SD) of three samples per time point. e) The heating curves of pure water and IR825–PEG solutions with different concentrations (0.05, 0.1, 0.2, and 0.5 mg mL^{-1}) under 808-nm laser irradiation at the power density of 0.5 W cm^{-2}. f) The heating curves of IR825–PEG and ICG solutions at the same concentration of 0.1 mg mL^{-1} under laser irradiation (808 nm, 0.5W cm^{-2}). g) UV-vis-NIR absorbance spectra of IR825–PEG (0.01 mg mL^{-1}) and ICG molecules (0.01 mg mL^{-1}) before and after 10 min of laser irradiation (808 nm, 0.5 W cm^{-2}, 10 min). Inset: Photos of IR825–PEG and ICG solutions before and after laser irradiation.

types of cells. The standard methyl thiazolyl tetrazolium (MTT) assay was carried out to determine the relative viabilities of 4T1 murine breast cancer cells, HeLa human epithelial carcinoma cells, and 293T human embryo kidney cells after they were incubated with IR825–PEG at various concentrations for 24 h and 48 h. No significant cytotoxicity of IR825–PEG was observed for all three types of cells even at high concentrations up to 0.2 mg mL^{-1} (**Figure 2**a,b). To further look for any potential cell damage caused by IR825–PEG nanoparticles, release of lactate dehydrogenase (LDH), an indicator of cell membrane damage, was also examined. It was found that the levels of released LDH from IR825–PEG incubated cells were normal compared to that of untreated cells, indicating no obvious cell membrane damage induced by IR825–PEG nanoparticles (Figure 2c). Reactive oxygen species (ROS) such as $\cdot O^{2-}$, $\cdot OH$, and H_2O_2 can damage biomacromolecules such as DNA, proteins, and lipids, resulting in a high degree of cytotoxicity. Herein, intracellular peroxide and superoxide levels in three types were assessed using a dihydroethidine (DHE) probe. No significant increase in the percentage of DHE positive cells after treatment with different concentrations of IR825–PEG nanoparticles was noticed, suggesting minimal oxidative stress induced to cells after IR825–PEG treatment (Figure 2d). In addition, we further collected primary mouse macrophage cells from healthy Blab/c mice, and tested the viabilities

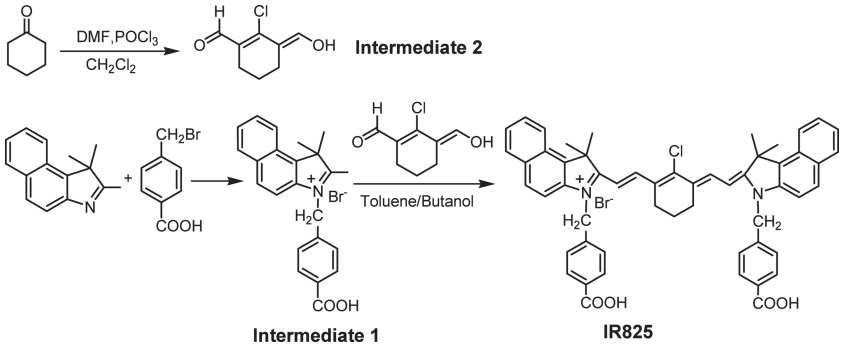

Scheme 1. A scheme showing the synthetic procedure for IR825.

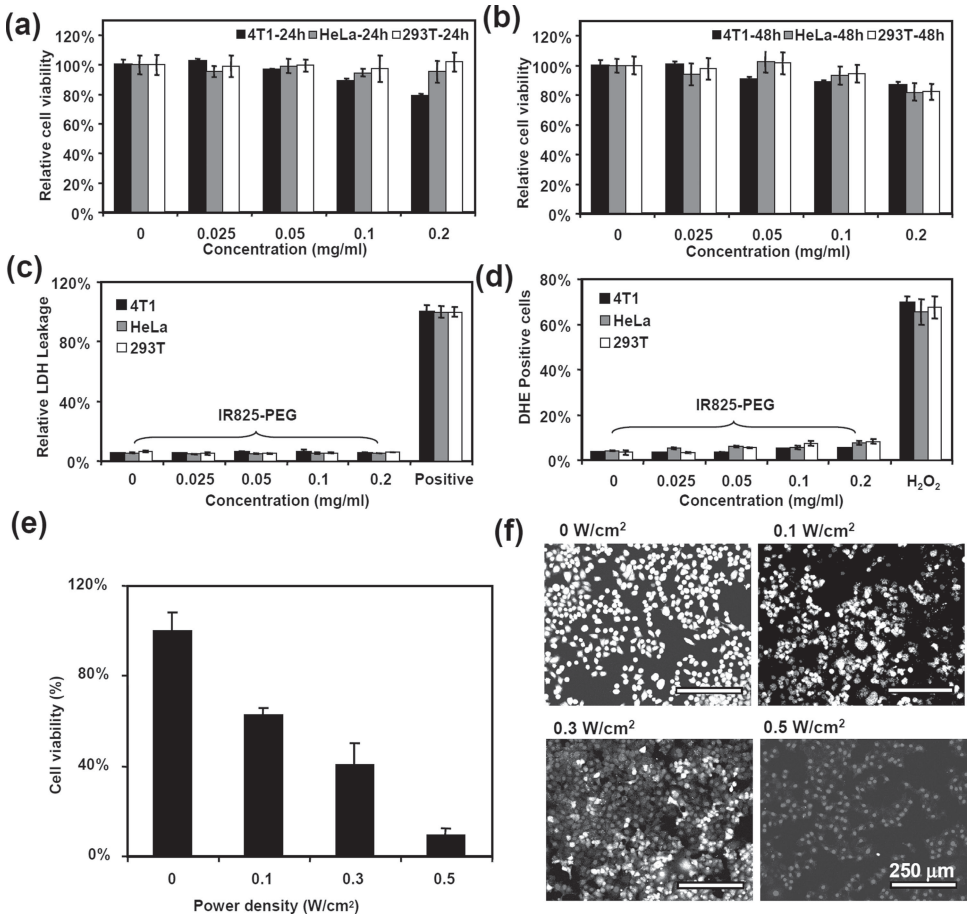

Figure 2. In vitro cell experiments. a,b) Relative viabilities of 4T1, HeLa, and 293T cells after being incubated with various concentrations of IR825–PEG a) for 24 h and b) 48 h. c) Levels of released LDH from three types of cells after being exposed to various concentrations of IR825–PEG. d) Generation of intracellular ROS determined by DHE staining and FACS measurement after various treatments indicated. Error bars were based on SD of three parallel samples at the minimum. e) Relative viabilities of 4T1 cells after IR825–PEG-induced photothermal ablation at different laser power densities. Error bars were based on the SD of six parallel samples. f) Confocal fluorescence images of calcein AM/PI co-stained 4T1 cells with IR825–PEG (25 μg mL^{-1}) incubation after being exposed to the 808-nm laser at different power densities. Live and dead cells were stained by Calcein AM and PI, and presented in white and dark gray colors in those images, respectively.

of those macrophages after incubation with IR825–PEG for 24 h (Supporting Information, Figure S5). No obvious toxicity of IR825–PEG was found toward primary macrophages, which play important roles in the immune system. Our data collectively suggest that IR825–PEG nanoparticles exhibit no appreciable toxicity to cells under our tested high concentrations.

Next, we used IR825–PEG nanoparticles as the photothermal agent for in vitro cancer cell ablation under laser irradiation. We first studied the cell uptake of fluorescently labeled IR825–PEG by confocal fluorescence microscope (Supporting Information, Figures S6,S7), and observed the efficient uptake of those nanoparticles by 4T1 cancer cells. For in vitro PTT study, 4T1 cells were incubated with IR825–PEG at the concentration of 20 μg mL^{-1} for 4 h and then irradiated by the 808-nm laser with different power densities. Following laser irradiation, the cells were co-stained by calcine AM and propidium iodide (PI) to differentiate live and dead cells, respectively, and imaged by a confocal fluorescence microscope (Figure 2f). An MTT assay was also performed to quantitatively measure the relative cell viabilities after PTT treatment under different laser powers (Figure 2e). It was determined that as the increase of laser power density, more cells incubated with IR825–PEG were killed after the laser irradiation. The majority of cells were destroyed after being incubated with 20 μg mL^{-1} of IR825–PEG and exposed to the NIR laser at 0.5 W cm^{-2} for 5 min. In contrast, cells without IR825–PEG incubation were not affected even after laser exposure at the highest tested power density (0.5 W cm^{-2}). These findings demonstrated that IR825–PEG nanoparticles hold great promise as an effective photothermal agent for in vivo tumor therapy.

For animal experiments, we first studied the blood circulation behavior of IR825–PEG nanoparticles. After i.v. injection of IR825–PEG into female Balb/c mice (1 mg mL^{-1}, 200 μL per mouse, or a dose of 10 mg kg^{-1}), blood was drown from the mouse tail at certain time intervals post injection (p.i.), solubilized by a lysis buffer, and then measured by a UV-vis-NIR spectrophotometer. The NIR absorbance peak of IR825 was employed to directly determine the IR825–PEG concentrations

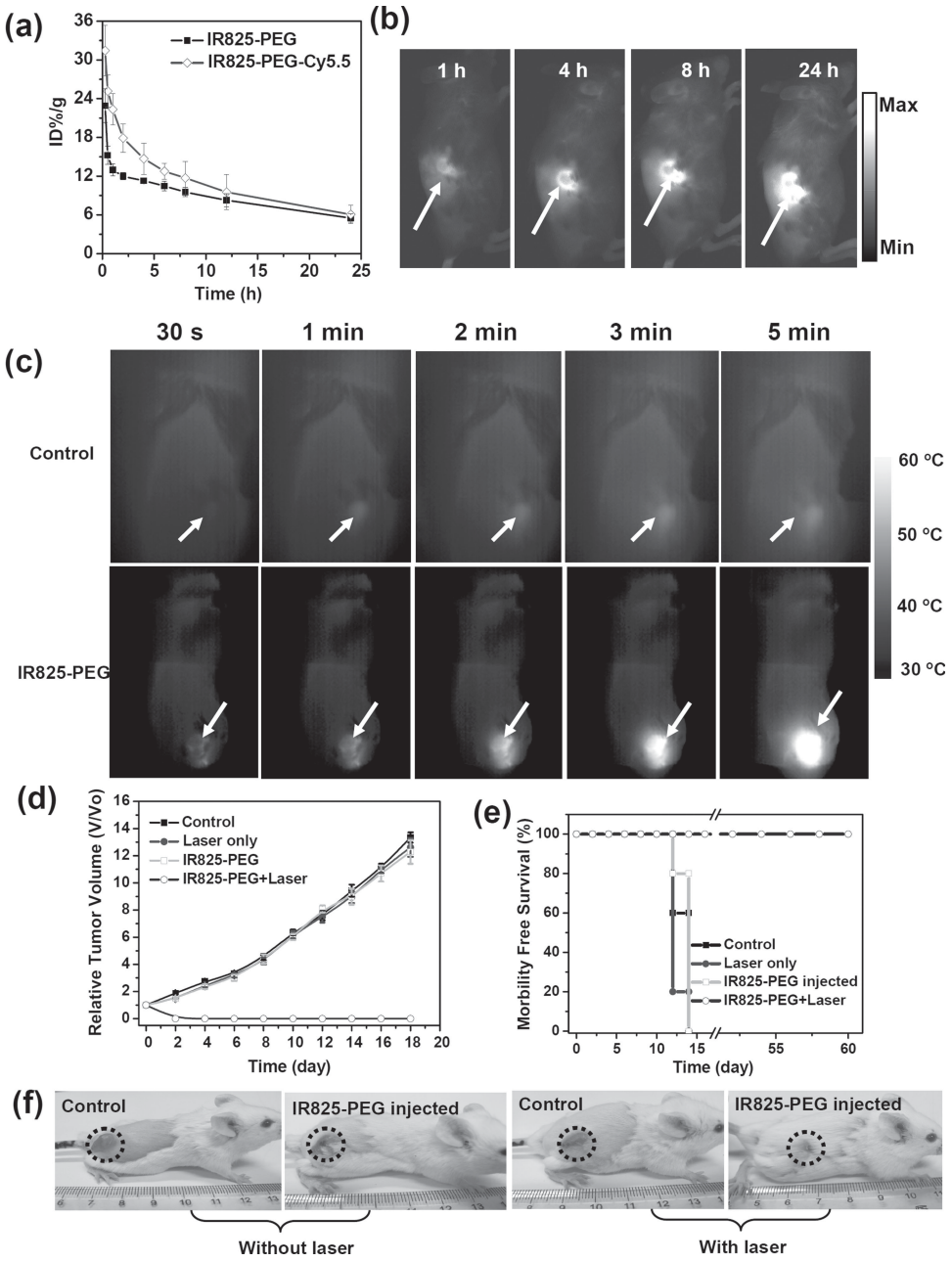

Figure 3. In vivo behavior and photothermal therapy. a) The blood circulation curves of IR825–PEG and IR825–PEG-Cy5.5 after i.v. injection as determined by measuring IR825 absorbance or Cy5.5 fluorescence, respectively, in the blood at different time points p.i. The unit was the percentage of injected dose per gram tissue (%ID/g). b) In vivo fluorescence images of 4T1 tumor bearing Balb/c mice at different time points post injection of IR825–PEG-Cy5.5. c) IR thermal images of 4T1 tumor-bear mice without (upper row) or with (lower row) intravenous injection IR825–PEG (10 mg kg^{-1}, 24 h p.i.) under the 808-nm laser irradiation taken at different time intervals. The laser power density was 0.5 W cm^{-2}. Arrows point to the tumors. d) The growth of 4T1 tumors in different groups of mice after various treatments indciated. The relative tumor volumes were normalized to their initial sizes. For the treatment group, six mice injected with IR825–PEG at 24 h p.i. were exposed to the 808-nm laser (0.5 W cm^{-2}, 5 min). Other three groups of mice were used as controls: untreated (Control, n = 6); laser only without IR825–PEG injection (laser only, $n = 6$); IR825–PEG injected but without laser irradiation (IR825-PEG only, $n = 6$). Error bars were based on SD. e) Survival curves of mice after various treatments as indicated in (d). f) Representative photos of mice after various different treatments indicated.

in blood samples (Supporting Information, Figure S8). It was uncovered that the blood circulation of IR825–PEG nanoparticles followed a typical two-compartment model. After a rapid decay with the first phase (distribution phase, usually a rapid decline) half-life of 0.99 h ± 0.26 h, those nanoparticles in the blood circulation exhibited an ultra-long second phase (elimination phase, the predominant process for drug clearance) half-life at 16.6 h ± 3.5 h (**Figure 3**a).

We then wanted to understand the in vivo distribution of IR825–PEG in mice. Because of the strong light scattering

in organ lysate samples, it was impossible to adopt the same method used for blood sample measurement to determine the concentrations of IR825–PEG in different organs after i.v. injection. Therefore, we used amine-terminated C18PMH-PEG to solubilize IR825, and then labeled IR825–PEG nanoparticles with Cy5.5, a commonly used NIR fluorescent dye (see Experimental Section for details and Supporting Information, Figure S6). The obtained IR825–PEG-Cy5.5 was also i.v. injected into mice at the same dose. The blood collected at different time points p.i. was solubilized by a lysis buffer and measured by a fluorometer to determine the IR825–PEG-Cy5.5 concentration based on Cy5.5 fluorescence. Different from directly measuring IR825 absorbance in blood samples, this fluorescent measurement approach as an indirect method is in fact measuring Cy5.5 conjugated on the PEG coating of IR825–PEG. Interestingly, the blood circulation data determined by these two different methods matched reasonably well with each other, suggesting that the PEG coating was stable in IR825–PEG nanoparticles when they were circulating in the blood after i.v. injection.

Since the Cy5.5 labeling on IR825–PEG nanoparticles was found to be fairly stable, we next used in vivo imaging approach to track IR825–PEG-Cy5.5 in mice after injection. Balb/c mice bearing 4T1 murine breast cancer tumors were intravenously injected with IR825–PEG-Cy5.5 (200 μL of 1 mg mL^{-1} solution for each mouse) and then imaged by a Maestro EX in vivo fluorescence imaging system (CRi, Inc.). The mouse autofluorescence was removed by spectral unmixing using the Maestro software, leaving pure Cy5.5 fluorescence shown in Figure 3b. It was found that IR825–PEG-Cy5.5 tended to be enriched in the tumor over time, with prominent uptake observed in the tumor at 24 h p.i. The high tumor accumulation of IR825–PEG nanoparticles could be due to the EPR effect in cancerous tumors with tortuous and leaky vasculatures, which tend to trap nanomaterials especially those with long blood circulation time.[22,35] Those mice were then sacrificed at 24 h p.i., with major organs collected and homogenized by a lysis buffer. Based on the intensity of Cy5.5 fluorescence, high levels of IR825–PEG-Cy5.5 were observed in the tumor, as well as in reticuloendothelial systems (RES) such as liver and spleen (Supporting Information, Figure S9). The tumor uptake was measured to be as high as 22.5% ID g^{-1}. However, it should be aware that the quantitative biodistribution data of IR825–PEG-Cy5.5 based on Cy5.5 labeling may not be entirely accurate, and a precise approach to directly measure IR825 levels in different organs and tissues remain to be developed in future studies, as the fluorescence of IR825 itself is rather weak.

Encouraged by the high tumor accumulation of IR825–PEG nanoparticles and its strong NIR optical absorption, we then carried out an in vivo photothermal therapy experiment using IR825–PEG. After being intravenously injected with IR825–PEG solutions (1 mg mL^{-1}, 200 μL for each mouse) for 24 h, mice bearing 4T1 tumors were anesthetized and exposed to an 808-nm laser at the power density of 0.5 W cm^{-2}. An infrared (IR) thermal mapping apparatus was used to record the temperature change in the tumor area under NIR irradiation. From mice i.v. injected with IR825–PEG, their tumor surface temperature rapidly increased from ≈30 °C to ≈60 °C within 5 min of laser irradiation (Figure 3c). In comparison, the tumor temperature on mice without IR825–PEG injection under the same irradiation condition showed little change.

Finally, the in vivo therapeutic efficacy of IR825–PEG induced PTT cancer treatment was studied. Six mice bearing 4T1 tumors with the average volume of ≈60 mm^3 on their back were i.v. injected with IR825–PEG (200 μL, 1 mg mL^{-1}). At 24 h p.i., the tumor of each mouse in the treatment group was exposed to the 808-nm laser at a power density of 0.5 W cm^{-2} for 5 min. Three other groups including untreated mice (control, $n = 6$), mice exposed to the laser (laser only, $n = 6$), and IR825–PEG injected mice without laser irradiation (IR825–PEG, $n = 6$), were used as the controls (with the average tumor volume at ≈60 mm^3). Tumor sizes were measured every 2 days after treatment. Remarkably, tumors on IR825–PEG injected mice were completely eliminated one-day post NIR laser irradiation (Figure 3d,f). In marked contrast, neither laser irradiation at this power density nor IR825–PEG injection by itself would affect the tumor development (Figure 3d). While mice in the three control groups showed average life spans of 16–18 days with the tumor volumes reached up to ≈1.0 cm^3, mice in the treated group (IR825–PEG +Laser) were tumor-free after treatment and survived over 60 days without a single death (Figure 3e,f). Our results suggest that IR825–PEG is a powerful agent for in vivo photothermal ablation of cancer.

Despite the absence of obvious in vitro toxicity of IR825–PEG to a number of different cell lines, its potential in vivo toxicity to animals is still an important question to be addressed. We carefully supervised the behaviors of IR825–PEG injected (10 mg kg^{-1}) Balb/c mice in our experiments after photothermal tumor ablation, and noticed no obvious sign of toxic effect within 60 days. No abnormalities in body weight (Supporting Information, Figure S10), eating, drinking, grooming, activity, exploratory behavior, urination, or neurological status were observed. Mice were then sacrificed at day 60 for careful necropsy, which uncovered no appreciable abnormality in major organs. Major organs of mice were sliced and stained by hematoxylin and eosin (H&E) for histology analysis (**Figure 4**a), revealing no noticeable organ damage or inflammatory lesion in all major organs of mice 60 days after PTT treatment.

To further understand the potential toxicology of IR825–PEG nanoparticles in relatively short and long terms, serum biochemistry assay and complete blood count were carried on IR825–PEG injected (10 mg kg^{-1}) healthy Balb/c mice at 1, 7, and 40 days p.i. The liver function markers including alanine aminotransferase (ALT), alkaline phosphatase (ALP), aspartate aminotransferase (AST), as well as kidney function marker urea nitrogen (BUN) and the albumin/globin ratio, were all measured to be normal (Figure 4b–d), suggesting no obvious hepatic or kidney disorder of mice induced by IR825–PEG treatment. A complete blood count assay was also carried out. Compared with the control group, all parameters including white blood cells (WBC), red blood cells (RBC), hematocrit (HCT), hemoglobin (Hgb), mean corpuscular volume (MCV), mean corpuscular hemoglobin (MCH), mean corpuscular hemoglobin concentration (MCHC), and platelets, were normal and within the reference ranges for healthy Balb/c mice (Figure 4e). Our results collectively evidence that IR825–PEG is not noticeably toxic in vivo to mice at our tested dose, although future careful

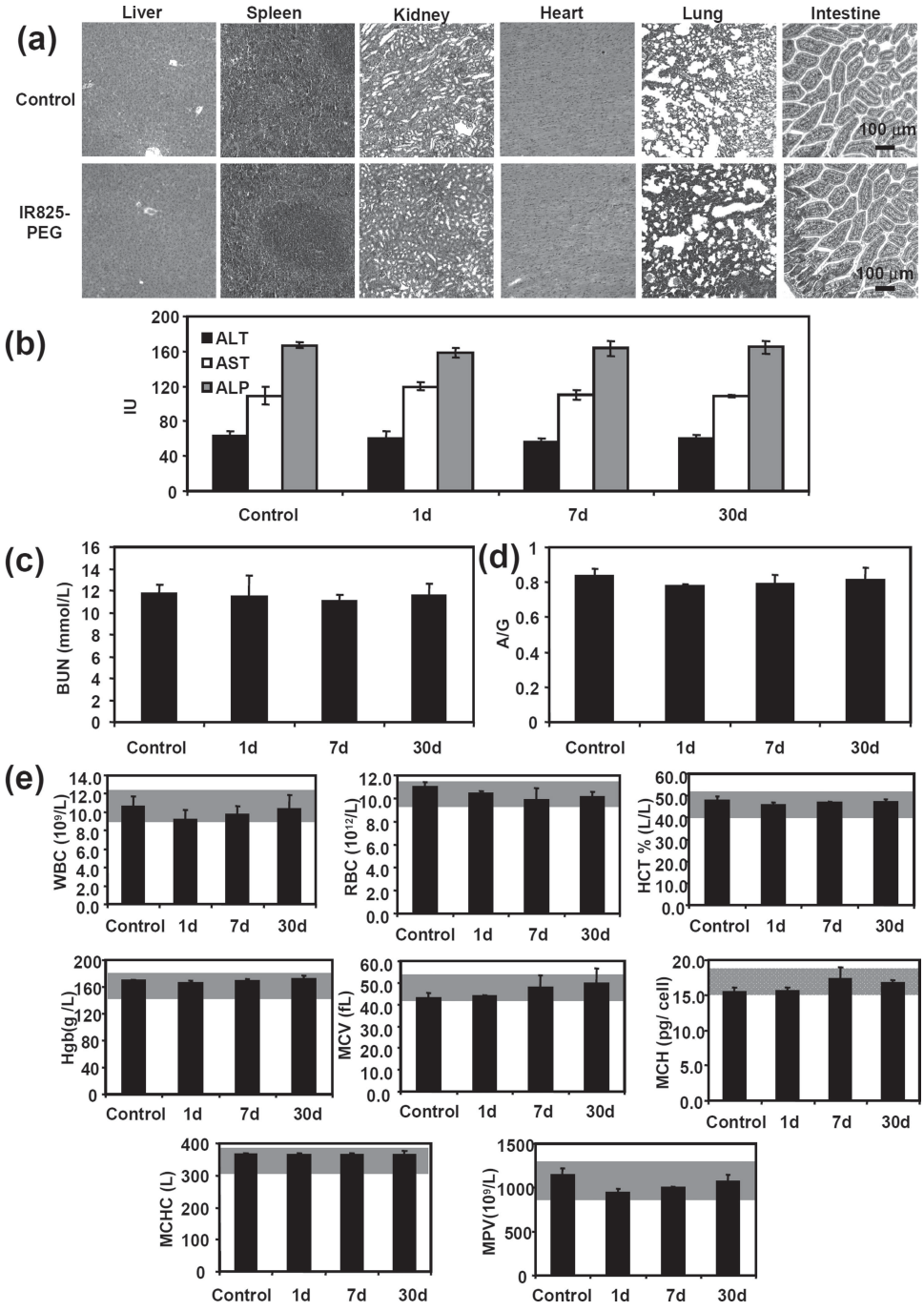

Figure 4. In vivo toxicology study. a) H&E stained images of major organs. IR825–PEG injected mice that survived after PTT (with tumors eliminated) were sacrificed 60 days after treatment. Untreated healthy mice were used as the control. No noticeable abnormality was observed in major organs including, liver, spleen, kidney, heart, and lung. b) Serum biochemistry data including liver function markers, c) blood urea nitrogen (BUN) levels, and d) albumin/globin ratios. Healthy female Balb/c mice i.v. injected with IR825–PEG (dose = 10 mg kg^{-1}) were sacrificed at 1, 7, and 40 days p.i. for blood collection. Untreated healthy mice were used as the control. e) Complete blood counts. Blood levels of WBC, RBC, HCT, Hgb, MCV, MCH, MCHC, and platelets of control and IR825–PEG treated mice were measured. Gray areas indicate the reference normal ranges for healthy female Balb/c mice. Statistic was based on 5 mice per data point.[38]

studies are still required to systematically examine any potential long-term toxicity of our IR825–PEG nanoparticles at various doses to animals, before any possible clinical use of this new organic photothermal agent. Moreover, we still need to develop a reliable approach to extract and quantitatively measure IR825 in different organs of mice after injection, so that we could understand the possible degradation and excretion behaviors of IR825–PEG in vivo.

3. Conclusions

We have successfully developed a new generation of photothermal therapeutic agent based on PEGylated micelle nanoparticles of a NIR-absorbing low-QY organic dye, IR825. It is found that IR825–PEG nanoparticles exhibit excellent compatibility in physiological environments, show no observable toxicity to three classes of cells at the tested concentrations, and can be used as a highly effective photothermal agent with remarkably improved photostability in comparison to ICG. With a long blood circulation half-life, the IR825–PEG nanoparticles show surprisingly high in vivo tumor uptake by the EPR effect after i.v. injection, and appear to be an excellent PTT agent for tumor ablation under a low-power laser irradiation, without rendering any appreciable toxicity to the treated animals. Although at the current stage we do not have direct data to study the degradation behaviors of IR825–PEG nanoparticles in vivo, those PEGylated micelles encapsulating small organic dye molecules likely could be slowly degraded in biological systems, and may have much less concern regarding their potential long-term toxicity in comparison to various inorganic photothermal agents as well as organic conjugated polymers. On the other hand, the dose (10 mg kg^{-1}) and optical power density (0.5 W cm^{-2}) used in our work are rather low in comparison to those used in a lot of other reported photothermal cancer treatment studies by systemic administration (e.g., laser power densities at 2–4 W cm^{-2} are needed for gold nanorods and nanoshells at similar doses),[39,40] suggesting that our IR825–PEG nanoparticles show comparable, if not better, photothermal therapeutic efficacy compared to many types of existing photothermal agents. Although further careful studies are required to understand the detailed biodistribution, pharmacokinetics, and long-term dose-dependent toxicology of IR825, it is expected the development of organic photothermal agents such as that presented in this study may be a reasonable approach to make photothermal therapy a clinically acceptable therapeutic method.

4. Experimental Section

Synthesis of Heptamethine Indocyanine Dye IR825:[41–43] The procedure of synthesizing IR825 is illustrated in Scheme 1. In brief, 2,3,3-trimethyl-4,5-benzo-3H-indole (TMBI, 10.0 g, 48 mmol) and alpha-bromo-p-toluic acid (BTA, 12.3 g, 57 mmol) were dissolved in 40 mL dichlorobenzene and stirred under 110 °C for 4 h. The solid crude product was then filtrated and recrystallized in methanol. The purified product as denoted intermediate 1 was dried under vacuum.

80 mL DMF/dichloromethane mixture (1/1, v/v) was added dropwisely into a solution of phosphoryl chloride (37 mL) and anhydrous dichloromethane (35 mL) under stirring in ice/water bath; afterwards, 10 g cyclohexanone was added dropwisely. The ice/water bath was removed and the solution was then heated and refluxed for 3 h. The mixture was poured into ice, yielding a solid product which was collected by filtration and washed with iced diethyl ether. The resulting yellow product was denoted as intermediate 2 and used directly.

Intermediate 1 (1.64 g, 3.9 mmol) and intermediate 2 (0.34 g, 1.9 mmol) were mixed in 260 mL butanol/toluene (7/3, v/v), and stirred for 4 h under 115 °C. The solvent was removed by rotatory evaporation, and the crude product was purified by dissolving in DMF and precipitating in diethyl ether. After filtration, the product was dried under vacuum.

Synthesis C_{18}PMH–PEG and C_{18}PMH–PEG–NH_2: C18PMH–PEG was synthesized following a literature procedure.[36] 10 mg (1 eq) poly(maleic anhydride-alt-1-octadecene) (C18PMH, Sigma-Aldrich) and 143 mg (1 eq) mPEG-NH_2(5K) (Biomatrik, Jiaxing, China) were dissolved in 5 mL dichloromethane with 6 µL triethylamine (TEA, Sinopharm Chemical Reagent Co.) and 11 mg 1-ethyl-3-(3-dimethylaminopropyl) carbodiimide (EDC, Fluka) added. After 24 h of stirring, the dichloromethane solvent was blowing-dried by N_2. The leftover solid was dissolved in water, forming a transparent clear solution, which was dialyzed against distilled water for 2 days in a dialysis bag with molecular weight cut-off (MWCO) of 14 kDa to remove unreacted mPEG–NH_2. After lyophilization, the final product was stored at –20 °C for future use.

To synthesize C_{18}PMH–PEG–NH_2, 10 mg (1 eq) C_{18}PMH, 95 mg (0.67 eq) mPEG–NH2(5k), and 48 mg (0.33 eq) NH_2–mPEG(5k)–BOC (Polymere, Germany) were mixed together in dichloromethane under agitation to form a homogeneous solution, EDC(2 eq) and TEA (8 eq) were then added under magnetic stirring. After stirring for 24 h at room temperature, the dichloromethane solvent was blowing-dried by N_2. Subsequently, 2 mL trifluoroacetic acid (TFA, Sinopharm Chemical Reagent Co.) was added under magnetic stirring for 3 h at room temperature to de-protect the Boc group. After evaporating the TFA solvent, the leftover solid was dissolved in water, and dialyzed for 2 days in a dialysis bag (MWCO 14 kDa) to remove unreacted PEG polymers and other reagents. After lyophilization, the final product (C18PMH–PEG–NH_2) was stored at –20 °C for future use.

Formation of IR825–PEG Nanoparticles: 20 mg as-synthesized IR825 was first dispersed in 5 mL methanol containing 20 mL TEA. Another solution of 100 mg C18PMH–PEG or C18PMH–PEG–NH_2 polymer in 2 mL methanol was then added to the reaction vessel. The mixture was stirred for 4 h before it was transferred into 5 mL water. The IR825–PEG nanoparticles were obtained after dialyzing the solution for 2 days in a dialysis bag (MWCO 14 kDa) to remove TEA and other reagents. The encapsulation efficiency of IR825 by C18PMH–PEG was nearly 100%, as evidenced by the fact that the filtrate was completely colorless even after a long period of dialysis.

Photothermal Stability Test: Aqueous solutions of IR825–PEG and ICG (0.1 mg mL^{-1}) in two 35-mm cell culture dishes were exposed to the 808-nm laser at the power density of 0.5 W cm^{-2} for 10 min. Photos and UV-vis-NIR spectra of those two solutions before and after laser irradiation were recorded and presented in Figure 1g.

Fluorescent Labeling of IR825–PEG: C_{18}PMH–PEG–NH_2 was used to solubilize IR825 in this case, yielding IR825–PEG–NH_2 with amino groups at PEG terminals. The purified IR825–PEG–NH_2 (0.5 mg mL^{-1}) was reacted with an amine reactive dye, Cy5.5–NHS (Passkey Technology Co., Ltd. Hunan China) at 0.1 mg mL^{-1} in a pH 7.4 phosphate buffer (0.02 M). After overnight stirring at room temperature in a light-proof container, the obtained IR825–PEG–Cy5.5 was purified by centrifugal filtration through 100 kDa MWCO filters and repeated water washing until no noticeable Cy5.5 color in the filtrate solution.

Characterization: Fluorescence spectra of different samples were obtained on a FluoroMax 4 luminescence spectrometer (HORIBA Jobin Yvon). UV-vis-NIR absorbance spectra were recorded by using a PerkinElmer Lambda 750 UV-vis-NIR spectrophotometer. AFM images were acquired using a Multi-Mode V Atomic forcemicroscopy (AFM, Veeco). TEM was performed using a FEI 20 TEM operated at an accelerating voltage of 200 kV. The samples were stained with phosphotungstic acid (1 wt%) before TEM imaging.

Cell Culture Experiments: 4T1 murine breast cancer cells, human cervical cancer HeLa cells, and 293T human embryo kidney cells were cultured in standard cell media recommended by American type culture collection (ATCC), under 37 °C within 5% CO_2 atmosphere.

Cells seeded into 96 well plates were incubated with different concentrations of IR825–PEG for 24 h. Relative cell viabilities were determined by the standard MTT assay. For in vitro photothermal therapy, 4T1 cancer cells were incubated with and without IR825–PEG (25 µg mL^{-1}) for 4 h and then irradiated by an 808-nm laser at different power densities (0.1, 0.3, 0.5, 0.8 W cm^{-2}) for 5 min. The cells were stained with Calcine AM/PI for 30 min, washed with PBS, and then imaged by a confocal fluorescence microscope (Leica).

The LDH leakage was measured using a cytotoxicity detection kit (Promega Cat. 7891) following the vendor's protocol. In this experiment, 4T1, HeLa, and 293T cells lysed by 1% Triton-X-100 were used as positive controls, while the cell-free medium was used as the negative control. The analysis was performed using a microplate reader (Bio-Rad).

ROS production was evaluated by a hydroethidine (DHE) probe known be oxidized by various oxidative agents. In brief, cells were treated with different concentrations of IR825–PEG for 24 h. After trypsination, cells were centrifuged at 1000 min r^{-1} for 3 min, re-suspended in cell culture medium containing 1 μM DHE (sigma), and analyzed using a flow cytometry (FACS Calibur from Becton, Dickinson and Company).

Tumor Model: Balb/c mice were obtained from Suzhou Belda Bio-Pharmaceutical Co., Ltd. and used under protocols approved by Soochow University Laboratory Animal Center. The 4T1 tumors were generated by subcutaneous injection of 2×10^6 cells in ≈40 μL serum-free RMPI-1640 medium onto the back of each female Balb/c mice.

In Vivo Fluorescence Imaging: 4T1 tumor bearing mice were intravenously injected with 200 μL of 1 mg mL^{-1} IR825–PEG–Cy5.5 and imaged using the Maestro in vivo fluorescence imaging system (CRi Inc.), in vivo spectral imaging from 650 nm to 800 nm (10 nm step) was carried out (central excitation wavelength = 640 nm) with an exposure time of 100 ms for each image frame. Auto-fluorescence (particularly from food residues in the stomach and intestine) was removed by using the spectral unmixing software.

Blood Circulation: Blood circulation was measured by drawing ≈10 μL blood from the mouse tail vein post injection of IR825–PEG or IR825–PEG–Cy5.5. Each blood sample was dissolved in 1 mL of lysis buffer (1% SDS, 1% Triton X-100, 40 mM Tris Acetate) to form a homogenous clear solution. The concentrations of IR825–PEG in the blood lysates were determined by the UV-vis spectra IR825 absorbance. A blank blood lysate sample without IR825–PEG was measured to determine the base-absorption level from red blood cells, which was subtracted from the measured IR825 absorbance at 825 nm of blood samples collected from IR825–PEG injected mice for the concentration calculation (Supporting Information, Figure S5). The IR825–PEG level in the blood was presented as the percentage of injected dose per gram tissue (% ID g^{-1}).

For IR825–PEG-Cy5.5 injection, the blood circulation was determined by the fluorescence spectra. A blank blood sample without IR825–PEG–Cy5.5 was measured to determine the blood auto-fluorescence level, which was also subtracted from the Cy5.5 fluorescence intensities of injected samples during the concentration calculation.

Biodistribution Measurement: For biodistribution study, 4T1 tumor-bearing mice were sacrificed at 24 h post injection of IR825–PEG–Cy5.5. The organs/tissues were weighed and homogenized in the lysis buffer (the same as the above used in blood circulation experiment) with a PowerGen homogenizer (Fisher Scientific). Clear homogenous tissue solutions were obtained and diluted by 10–100 times to avoid significant light scattering and self-quenching during fluorescence measurement. The fluorescence intensities of both standard samples and real tissue samples were all adjusted to be in the linear range by appropriate dilution. The samples were triplicatedly measured to insure reproducibility and measurement accuracy. The biodistribution of IR825–PEG–Cy5.5 based on Cy5.5 fluorescence in various organs of mice was then calculated and plotted in unit of % ID g^{-1}.

In Vivo Photothermal Therapy: An optical fiber coupled 808-nm high power diode-laser (Hi-Tech Optoelectronics Co., Ltd. Beijing, China) was used to irradiate tumors during our experiments. For photothermal treatment, the laser beam with a diameter of ≈10 mm was focused on the tumor area at the power density of 0.5 W cm^{-2} for five minutes. Infrared thermal images were taken by IRS E50 Pro Thermal Imaging Camera. The tumor sizes were measured by a caliper every the other day and calculated as the volume = ((tumor length) × (tumor width))^2/2. Relative tumor volumes were calculated as V/V_0 (V_0 is the tumor volume when the treatment was initiated).

Histology Analysis: 60 days after injection of IR825–PEG (dose = 10 mg kg^{-1}), 3 mice from the treatment group and 3 age-matched female Balb/c control mice (without any injection of IR825–PEG) were sacrificed by CO_2 asphyxiation for necropsy. Major organs from those mice were harvested, fixed in 10% neutral buffered formalin, processed routinely into paraffin, sectioned at 8 micrometers, stained with hematoxylin and eosin (H&E) and examined by a digital microscope (Leica QWin). Examined tissues include liver, spleen, kidney, heart, lung, and intestine.

Blood Analysis: Fifteen healthy Balb/c mice were injected with 200 μL of 1 mg mL^{-1} IR825–PEG (a dose of 10 mg kg^{-1}). Other five mice were used as the un-treated control. Mice were sacrificed to collect the blood (0.8 mL) for blood biochemistry assay and complete blood count at 1 day, 7 days, and 30 days post injection of IR825–PEG (five mice per group). The serum chemistry data and complete blood count were measured in Shanghai Research Center for Biomodel Organism.

Supporting Information

Supporting Information of IR825 characterization data, biodistribution data, and body weight data (after treatment) is available from the Wiley Online Library or from the author.

Acknowledgements

This work was partially supported by the National Natural Science Foundation of China (51222203, 51002100, 51132006), the National "973" Program of China (2011CB911002, 2012CB932601), and a Project Funded by the Priority Academic Program Development of Jiangsu Higher Education Institutions. L.C. was supported by a Post-doctoral research program of Jiangsu Province (1202044C).

Received: March 26, 2013
Revised: April 29, 2013
Published online: June 13, 2013

[1] S. Lal, S. E. Clare, N. J. Halas, *Acc. Chem. Res.* **2008**, *41*, 1842.
[2] J. T. Robinson, S. M. Tabakman, Y. Liang, H. Wang, H. S. Casalongue, D. Vinh, H. Dai, *J. Am. Chem. Soc.* **2011**, *133*, 6825.
[3] Y. Xia, W. Li, C. M. Cobley, J. Chen, X. Xia, Q. Zhang, M. Yang, E. C. Cho, P. K. Brown, *Acc. Chem. Res.* **2011**, *4*, 914.
[4] L. Dykman, N. Khlebtsov, *Chem. Soc. Rev.* **2012**, *41*, 2256.
[5] E. Boisselier, D. Astruc, *Chem. Soc. Rev.* **2009**, *38*, 1759.
[6] H. Ke, J. Wang, Z. Dai, Y. Jin, E. Qu, Z. Xing, C. Guo, X. Yue, J. Liu, *Angew. Chem. Int. Ed.* **2011**, *50*, 3017.
[7] H. Liu, T. Liu, X. Wu, L. Li, L. Tan, D. Chen, F. Tang, *Adv. Mater.* **2012**, *24*, 755.
[8] L. Cheng, K. Yang, Y. Li, J. Chen, C. Wang, M. Shao, S.-T. Lee, Z. Liu, *Angew. Chem. Int. Ed.* **2011**, *50*, 7385.
[9] W. Dong, Y. Li, D. Niu, Z. Ma, J. Gu, Y. Che, W. Zhao, X. Liu, C. Liu, J. Shi, *Adv. Mater.* **2011**, *23*, 5392.
[10] K. Yang, S. Zhang, G. Zhang, X. Sun, S.-T. Lee, Z. Liu, *Nano Lett.* **2010**, *10*, 3318.
[11] K. Yang, L. Feng, X. Shi, Z. Liu, *Chem. Soc. Rev.* **2013**, *42*, 530.
[12] C. Li, S. Bolisetty, K. Chaitanya, J. Adamcik, R. Mezzenga, *Adv. Mater.* **2013**, *3*, 1010.
[13] X. Huang, S. Tang, X. Mu, Y. Dai, G. Chen, Z. Zhou, F. Ruan, Z. Yang, N. Zheng, *Nat. Nanotechnol.* **2011**, *6*, 28.
[14] S. Tang, X. Huang, N. Zheng, *Chem. Commun.* **2011**, *47*, 3948.
[15] Q. Tian, M. Tang, Y. Sun, R. Zou, Z. Chen, M. Zhu, S. Yang, J. Wang, J. Hu, *Adv. Funct. Mater.* **2011**, *23*, 3542.
[16] Q. Tian, F. Jiang, R. Zou, Q. Liu, Z. Chen, M. Zhu, S. Yang, J. Wang, J. Wang, J. Hu, *ACS Nano* **2011**, *5*, 9761.
[17] Z. Chen, Q. Wang, H. Wang, L. Zhang, G. Song, L. Song, J. Hu, H. Wang, J. Liu, M. Zhu, D. Zhao, *Adv. Mater.* **2013**, *25*, 2095.
[18] S. Sharifi, S. Behzadi, S. Laurent, M. L. Forrest, P. Stroeve, M. Mahmoudi, *Chem. Soc. Rev.* **2012**, *41*, 2323.

[19] J. Yang, J. Choi, D. Bang, E. Kim, E.-K. Lim, H. Park, J.-S. Suh, K. Lee, K.-H. Yoo, E.-K. Kim, Y.-M. Huh, S. Haam, *Angew. Chem. Int. Ed.* **2011**, *50*, 441.
[20] K. Yang, H. Xu, L. Cheng, C. Sun, J. Wang, Z. Liu, *Adv. Mater.* **2012**, *24*, 5586.
[21] M. Chen, X. Fang, S. Tang, N. Zheng, *Chem. Commun.* **2012**, *48*, 8934.
[22] L. Cheng, K. Yang, Q. Chen, Z. Liu, *ACS Nano* **2012**, *6*, 5605.
[23] C. S. Jin, J. F. Lovell, J. Chen, G. Zheng, *ACS Nano* **2013**, *7*, 2541.
[24] C. Wang, H. Tao, L. Cheng, Z. Liu, *Biomaterials* **2011**, *32*, 6145.
[25] G. Fu, W. Liu, S. Feng, X. Yue, *Chem. Commun.* **2012**, *48*, 11567.
[26] Y. Liu, K. Ai, J. Liu, M. Deng, Y. He, L. Lu, *Adv. Mater.* **2013**, *25*, 1353.
[27] S. Luo, E. Zhang, Y. Su, T. Cheng, C. Shi, *Biomaterials* **2011**, *32*, 7127.
[28] X. Zheng, D. Xing, F. Zhou, B. Wu, W. R. Chen, *Mol. Pharmaceutics* **2011**, *8*, 447.
[29] C. Zheng, M. Zheng, P. Gong, D. Jia, P. Zhang, B. Shi, Z. Sheng, Y. Ma, L. Cai, *Biomaterials* **2012**, *33*, 5603.
[30] A. D. l. Zerda, S. Bodapati, R. Teed, S. N. Y. May, S. M. Tabakman, Z. Liu, B. T. Khuri-Yakub, X. Chen, H. Dai, S. S. Gambhir, *ACS Nano* **2012**, *6*, 4694.
[31] J. Yu, D. Javier, M. A. Yaseen, N. Nitin, R. Richards-Kortum, B. Anvari, M. S. Wong, *J. Am. Chem. Soc* **2010**, *132*, 1929.
[32] C. Kim, C. Favazz, L. V. Wang, *Chem. Rev.* **2010**, *110*, 2756.
[33] M. Zheng, C. Yue, Y. Ma, P. Gong, P. Zhao, C. Zheng, Z. Sheng, P. Zhang, Z. Wang, L. Cai, *ACS Nano* **2013**, *7*, 2056.
[34] X. Peng, H. Chen, D. R. Draney, W. Volcheck, A. Schutz-Geschwender, D. M. Olive, *Anal. Biochem.* **2009**, *388*, 220.
[35] G. Prencipe, S. M. Tabakman, K. Welsher, Z. Liu, A. P. Goodwin, L. Zhang, J. Henry, H. J. Dai, *J. Am. Chem. Soc* **2009**, *131*, 4783.
[36] X. Liu, H. Tao, K. Yang, S. Zhang, S.-T. Lee, Z. Liu, *Biomaterials* **2011**, *32*, 144.
[37] L. Cheng, K. Yang, M. Shao, S.-T. Lee, Z. Liu, *J. Phys. Chem. C* **2011**, *115*, 2686.
[38] Reference ranges of hematology data of healthy female Balb/c mice were obtained from Charles River Laboratories: http://www.criver.com/ENUS/PRODSERV/BYTYPE/RESMODOVER/RESMOD/Pages/BALBcMouse.aspx, accessed: June **2013**.
[39] G. v. Maltzahn, J.-H. Park, A. Agrawal, N. K. Bandaru, S. K. Das, M. J. Sailor, S. N. Bhatia, *Cancer Res.* **2009**, *69*, 3892.
[40] A. M. Gobin, M. H. Lee, N. J. Halas, W. D. James, R. A. Drezek, J. L. West, *Nano Lett.* **2007**, *7*, 1929.
[41] X. Peng, F. Song, E. Lu, Y. Wang, W. Zhou, J. Fan, Y. Gao, *J. Am. Chem. Soc* **2005**, *127*, 4170.
[42] J. C. Vaughan, G. T. Dempsey, E. Sun, X. Zhuang, *J. Am. Chem. Soc* **2013**, *135*, 1197.
[43] K. Kundu, S. F. Knight, N. Willett, S. Lee, W. R. Taylor, N. Murthy, *Angew. Chem. Int. Ed.* **2009**, *48*, 299.